

Exploring steric and electronic parameters of biaryl phosphacycles

Jairus L. Lamola,^a Adedapo S. Adeyinka,^a Frederick P. Malan,^b Paseka T. Moshapo,^a Cedric W. Holzapfel,^a and Munaka Christopher Maumela^{*a,c}Received 00th January 20xx,
Accepted 00th January 20xx

DOI: 10.1039/x0xx00000x

Electronic and steric properties of the newly developed biaryl phosphacycles were quantified from various experimental and theoretical methods. These include user-friendly and rapid packages such as Solid-G, SambVca, and FindConeAngle for the unique steric parameterisation studies of phospho-selenides. Electronic descriptors derived from the ^{31}P - ^{77}Se coupling constants ($^1J_{\text{P-Se}}$), C-O stretching frequency (ν_{CO}), computed bond enthalpies (ΔE), and molecular electrostatic potentials (V_{min}) exhibited moderate to good correlations.

Introduction

Tertiary phosphines (PR_3) have proved to be ideal ligands for a large number of transition-metal catalysed transformations such as cross-coupling¹, hydrogenation², hydroformylation³, carbonylation^{4,5}, metathesis^{6,7}, as well as alkene oligomerisation⁸ and polymerisation⁹. The widespread application of phosphine ligands lies in their ability to stabilise metals in several oxidation states and geometries, as well as their ability to be easily tuned to radically change the identity and reactivity of catalysts.^{10,11} These attractive qualities of phosphines have contributed mainly towards studies of their stereoelectronic properties and have been reviewed by several authors.^{12–15} Attempts to quantify these ligand parameters have been successfully demonstrated by the pioneering work of Tolman's steric¹⁶ and electronic¹⁷ parameters. Building from the Tolman concept and other classical approaches^{18,19,28,20–27}, computational methods such as the molecular electrostatic potential (MESP)²⁹, Sterimol³⁰, SambVca³¹, and FindConeAngle³² have enabled facile parameterisation of ligands and thus found widespread application.^{33–42}

These methods have demonstrated the importance of investigating ligand properties to better understand their structure-activity correlation in homogenous catalysis. We have recently prepared and evaluated biaryl phosphacycles **1–3** in Suzuki-Miyaura cross-coupling reactions (Fig. 1).^{43–45} These ligands proved to be active in the coupling of a variety of substrates at ambient temperature and exhibited comparable

to superior efficacies when compared to closely related dialkylbiaryl phosphines **4–6** (Fig. 1).⁴³

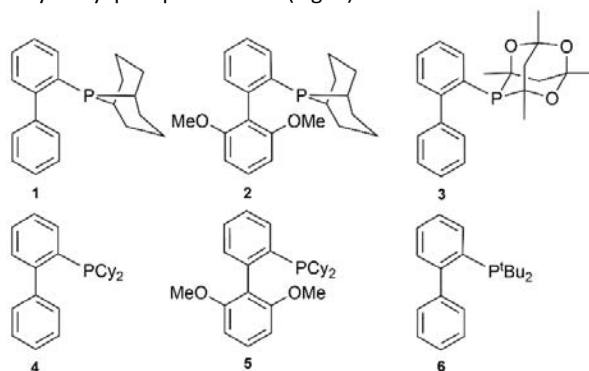


Fig. 1: Recently developed biaryl phosphacycles **1–3** and the well-established dialkylbiaryl phosphines **4–6**.

In this study, we investigated the electronic and steric properties of the biaryl phosphacycles **1–3**, dialkylbiaryl phosphines **4–6**, and PPh_3 (**7**) as a benchmark. To achieve this, a variety of experimental and theoretical approaches were explored (Fig. 2).

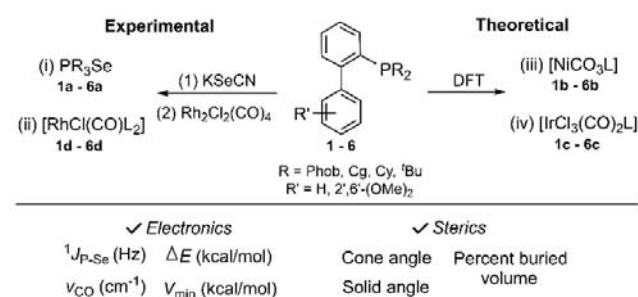


Fig. 2: Quantification of steric and electronic parameters of biaryl phosphines **1–6**.

We primarily focused on phospho-selenides which have been previously employed in the quantification of the electronic parameter of phosphine ligands through ^{31}P - ^{77}Se coupling constants ($^1J_{\text{P-Se}}$).^{15,21,23,46–52} This method was assessed and compared to classical approaches such as the C-O stretching

^a Research Centre for Synthesis and Catalysis, Department of Chemical Sciences, University of Johannesburg, Kingsway Campus, Auckland Park 2006, South Africa.

^b Department of Chemistry, University of Pretoria, Hatfield Campus, Hatfield 0002, South Africa.

^c Research and Technology, Group Technology, Sasol, 1 Klasie Havenga Rd, Sasolburg 1947, South Africa.

* chris.maumela@sasol.com

† Dedicated to the memory of Emeritus Professor Cedric Holzapfel (1935 – 2021).

We are eternally grateful for his mentorship and friendship.

‡ CCDC deposition numbers: 2051977, 2051921, 2051993, 2051992, 2051994, 2052006, 2120400-3. Electronic Supplementary Information (ESI) available, see DOI: 10.1039/x0xx00000x

frequency (ν_{CO}), bond enthalpy (ΔE), and molecular electrostatic potential (MESP) (Fig. 2). Most notable, we report the unprecedented application of biarylphospho-selenides in the quantification of steric parameters derived from the solid angle (Ω°), percent buried volume ($\% V_{\text{Bur}}$), and exact cone angle (θ°).⁵³

Results and discussion

Synthesis of phospho-selenides

The synthesis of phospho-selenides **1a** – **6a** and PPh_3Se (**7a**) was achieved by a one-step reaction of the free phosphines with KSeCN in a DCM/MeOH (1:1) solvent system, following modified literature protocols.^{48,54} The desired phospho-selenides were obtained in 87 – 95 % isolated yields. Following X-ray analysis, molecular structures of biarylphospho-selenides **1a** – **6a** and selected crystal crystallographic parameters are described (Fig. 3 and Table 1, respectively).

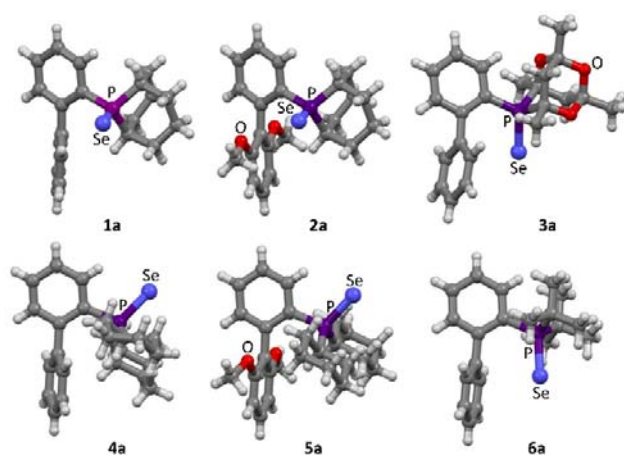


Fig. 3: X-ray structures (50% thermal ellipsoid probability) of biarylphospho-selenides derived from phobane[3.3.1] (Phob) (**1a** – **2a**), phosphatrioxa-adamantane (Cg) (**3a**), and dialkyl (Cy) (**4a** – **5a**) and (^tBu) (**6a**) moieties.

In general, the synthesised phospho-selenides exhibited $\text{P}=\text{Se}$

Table 1: Selected crystallographic and refinement parameters of phospho-selenides **1** – **7**.^a

PR_3Se^b	CCDC refcode	Empirical formula, _s	Crystal system, Z	Space group	R_1 index ^c
1a	2051977	$\text{C}_{40}\text{H}_{46}\text{P}_2\text{Se}_2$	triclinic, 2	$P-1$	0.0284
2a	2051921	$\text{C}_{22}\text{H}_{27}\text{O}_2\text{PSe}$	monoclinic, 4	$P2_1/c$	0.0552
3a	2051993	$\text{C}_{22}\text{H}_{25}\text{O}_3\text{PSe}$	monoclinic, 4	$P2_1/n$	0.0292
4a	2051992	$\text{C}_{24}\text{H}_{31}\text{PSe}$	monoclinic, 8	$C2/c$	0.0268
5a	2052006	$\text{C}_{26}\text{H}_{35}\text{O}_2\text{PSe}$	orthorhombic, 4	$Pna2_1$	0.0249
6a	2051994	$\text{C}_{40}\text{H}_{54}\text{P}_2\text{Se}_2$	monoclinic, 4	$P2_1/c$	0.0337
7a ^c	TPPHSE^{56}	$\text{C}_{36}\text{H}_{30}\text{P}_2\text{Se}_2$	monoclinic, 8	$P2_1/c$	0.0701

^aComplete crystallographic data and molecular structures can be retrieved from the ESI† (Table S2 – S5). ^bPhospho-selenides. ^cFinal R_1 index [$I \geq 2\sigma(I)$]. ^d PPh_3Se .

bond lengths between 2.123 Å and 2.099 Å (entries 1 – 7, Table 2). The shortest $\text{P}=\text{Se}$ bond length was exhibited by phospho-selenide **3a**, bearing the Cg moiety, which has been previously characterised by an electron-deficient phosphorus center.^{10,55} The described $\text{P}=\text{Se}-\text{C}_{\text{Ar}}$ bond angles (111.29° – 115.87°) suggests a tetrahedral geometry (entries 1 – 7, Table 2) as observed with the closely related phosphates.⁵⁷ The smallest biaryl torsional angles were exhibited by the unsubstituted biarylphospho-selenides **1a** and **4a** (entries 1 and 4), as opposed to the functionalised phospho-selenides **2a** and **5a** (entries 2 and 5), bearing the Phob and Cy moieties, respectively. The effect of substituents on the biaryl torsional angles has been previously reported.^{37,43} Most notable, phospho-selenides **3a** and **6a** exhibited the smallest $\text{Se}-\text{P}-\text{C}_{\text{q}}-\text{C}_{\text{q}}$ torsional angles (22.79° and 15.42° , entries 3 and 6, respectively), suggesting comparable structural features of the Cg and ^tBu moieties.¹⁰

Table 2. Selected bond lengths as well as bond- and torsion angles of phospho-selenides **1a** – **7a**.^a

Entry	PR_3Se^b	$\text{P}=\text{Se}$ (Å)	$\text{Se}-\text{P}-\text{C}_{\text{Ar}}$ ($^\circ$)	Torsional angle ($^\circ$)	
				Biaryl	$\text{Se}-\text{P}-\text{C}_{\text{q}}-\text{C}_{\text{q}}^c$
1	1a	2.1155(5)	113.08(6)	55.70(2)	95.58(15)
2	2a	2.1144 (13)	111.57(15)	75.90(6)	87.80(4)
3	3a	2.0994(4)	115.87(5)	73.30(2)	22.79(15)
4	4a	2.1215(4)	111.29(5)	70.47(19)	159.83(11)
5	5a	2.1230(7)	112.24(9)	88.70(3)	174.90(19)
6	6a	2.1102(5)	115.51(7)	79.10(3)	15.40(2)
7	7a	2.1060(1)	112.98(8)	-	-

^aComplete bond lengths, angles, and torsions can be retrieved from the ESI†.

^bPhospho-selenides. ^cTorsion generated between Se, P, and the neighbouring quaternary aromatic carbons.

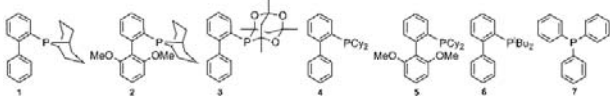
Quantification of steric parameters

Steric descriptors derived from phospho-selenides **1a** – **7a** were accessed from the computational programs SambVca⁵⁸, FindConeAngle³², and Solid-G²⁴, using default settings. The obtained steric descriptors are described in Table 4. The steric values determined from the crystallographic phospho-selenides **1a** – **7a** (entries 1 – 7), revealed an increase in steric bulk in the order **7a** < **1a** < **4a** < **5a** < **2a** < **3a** < **6a**. The observed trend for phospho-selenides derived from dialkylbiaryl phosphines (**4a** – **6a**) and PPh_3 (**7a**) was consistent with previous findings from metal complexes.^{33,42,59,60} Most notable, the previously reported $\% V_{\text{Bur}}$ of PPh_3 from the crystallographic $[\text{AuClPPh}_3]$ complex (29.9%)⁵⁹ was reproduced from phospho-selenide **7a** (entry 7, Table S18, ESI†). The larger steric values of biarylphospho-selenide **3a** (entry 3) compared to biarylphospho-selenide **1a** – **2a** (entry 1 – 2) correlates to steric indexing of diphosphines containing Phob and Cg moieties reported by Pringle and co-workers.⁶¹

Following previous studies on the quantification of steric parameters from theoretical structures,^{12,32,33,42} DFT structures of the phospho-selenides (**1a** – **7a**) were used to assess the generality of this study. Phospho-selenides **1a** – **7a** were fully optimised using B3LYP and ωB97xD functional with the 6-31+G, def2-TZVPP, and Lanl2DZ basis set, employing the Gaussian 09 rev E01 software⁶² (Table S8, ESI†). Through geometry comparisons, it was observed that the B3LYP-GD3/def2-TZVPP method yielded the most accurate DFT structures (Table S8, ESI†). Moreover, this enabled the

correlation of steric parameters derived from experimental and theoretical structures (entries 1 – 7, Table 3). The trend observed from steric indexing of crystallographic phospho-selenides **1a** – **7a** was reproduced from the corresponding DFT phospho-selenides **1aa** – **7aa**, and when plotted linear regressions with correlation factors (R^2) ranging from 0.9787 – 0.9944 exists (Fig. S1 – S3, ESI†).

Table 3: Steric parameterisation of biaryl phosphines **1** – **7** using the exact cone angles (ϑ°) of the corresponding experimental phospho-selenides ($\vartheta^\circ_{\text{Se-L}}$), and theoretical phospho-selenides ($\vartheta^\circ_{\text{Se-L}}^*$), $[\text{NiCO}_3\text{L}]$ ($\vartheta^\circ_{\text{Ni-L}}$), as well as $[\text{IrCl}_3(\text{CO})_2\text{L}]$ ($\vartheta^\circ_{\text{Ir-L}}$).^a



Entry	Ligand	Experimental		Theoretical	
		$\vartheta^\circ_{\text{Se-L}}$	$\vartheta^\circ_{\text{Se-L}}^*$	$\vartheta^\circ_{\text{Ni-L}}$	$\vartheta^\circ_{\text{Ir-L}}$
1	1	178.5	183.9 ^b	176.5	167.8
2	2	220.0	220.4	208.1	195.9 ^c
3	3	222.0	222.5 ^b	210.5	195.9
4	4	181.3	181.8	174.4	166.0
5	5	182.8	182.5	175.1	168.1
6	6	228.5	227.4	212.3	200.4
7	7	169.3	171.9 ^c	167.9	151.7

^aThe exact cone angles (ϑ) were quantified using FindConeAngle implemented in Mathematica.³² $\vartheta^\circ_{\text{Se-L}}$ is obtained from crystallographic data of phospho-selenides **1a** – **7a**. $\vartheta^\circ_{\text{Se-L}}^*$, $\vartheta^\circ_{\text{Ni-L}}$, and $\vartheta^\circ_{\text{Ir-L}}$ are obtained from theoretical DFT structures of phospho-selenides **1aa** – **7aa**, $[\text{NiCO}_3\text{L}]$ **1b** – **7b**, and $[\text{IrCl}_3(\text{CO})_2\text{L}]$ **1c** – **7c**, with the lowest average error (%) (Table S9 – S17, ESI†). The solid angle (Ω°) and percent buried volume (% V_{bur}) values are included in Table S18 (ESI†). Improved steric values can be obtained at ^bB3LYP/6-31+G, ^c ω B97xD/LanL2DZ, and ^dB3LYP-GD3/def2-TZVPP.

The closest correlation ($R^2 = 0.9944$) was observed from the comparison of the experimental and theoretical exact cone angles (ϑ°) (Fig. 4), obeying equation (1). Where $\vartheta^\circ_{\text{EXP.PSe}}$ and $\vartheta^\circ_{\text{THEOR.PSe}}$ represents experimentally and theoretically determined exact cone angles from phospho-selenides, respectively.

$$\vartheta^\circ_{\text{THEOR.PSe}} = 0.9480(\vartheta^\circ_{\text{EXP.PSe}}) + 11.403 \quad (1)$$

To further validate the use of phospho-selenides for quantification of steric parameters, correlations of this method to the well-established $[\text{NiCO}_3\text{L}]$ (**1b** – **7b**) and $[\text{IrCl}_3(\text{CO})_2\text{L}]$ (**1c** – **7c**) complexes are described in Table 3. DFT structures **1b** – **7b** and **1c** – **7c** were optimised at ω B97xD/LanL2DZ and B3LYP-GD3/def2-TZVPP levels of theory, and only those with the minimal average errors (%) are described (Table 3). In general, the trend previously described for phospho-selenides was observed with the $[\text{NiCO}_3\text{L}]$ and $[\text{IrCl}_3(\text{CO})_2\text{L}]$ complexes (Table 3). A good correlation was observed from comparing steric parameters of phospho-selenides **1a** – **7a** and $[\text{NiCO}_3\text{L}]$ **1b** – **7b** complexes with R^2 ranging from 0.9732 – 0.9902 (Fig. S4 – S9). A marginally lower R^2 range (0.9607 – 0.9790) was observed when steric parameters of phospho-selenides **1a** – **7a** were compared to those of $[\text{IrCl}_3(\text{CO})_2\text{L}]$ **1c** – **7c** complexes (Fig. S4 – S9). Similarly, the best linear correlation between phospho-selenides **1a**

– **7a** and metal complexes **1b** – **7b** as well as **1c** – **7c** was observed with the exact cone angle (ϑ°) (Fig. 4), following equations (2) and (3)

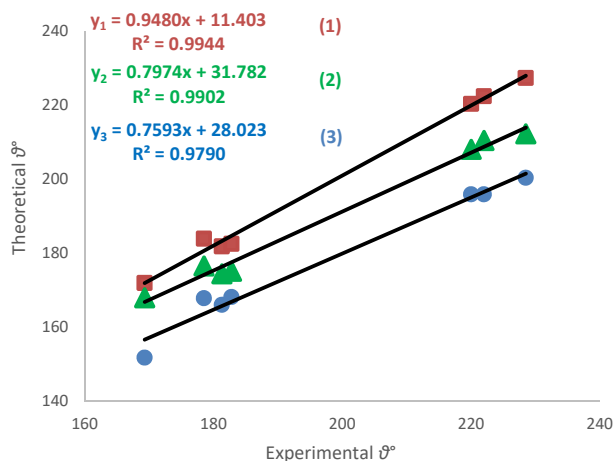


Fig. 4: Correlations between the exact cone angles (ϑ°) determined from crystallographic phospho-selenides **1a** – **7a** and theoretical phospho-selenides **1aa** – **7aa** (squares, y_1), $[\text{NiCO}_3\text{L}]$ **1b** – **7b** (triangles, y_2), and $[\text{IrCl}_3(\text{CO})_2\text{L}]$ **1c** – **7c** (circles, y_3) complexes.

, respectively. Where $\vartheta^\circ_{\text{EXP.PSe}}$, $\vartheta^\circ_{\text{THEOR.Ni/L}}$ and $\vartheta^\circ_{\text{THEOR.Ir/L}}$ represents the exact cone angles determined from experimental phospho-selenides and theoretical $[\text{NiCO}_3\text{L}]$ and $[\text{IrCl}_3(\text{CO})_2\text{L}]$ complexes, respectively.

$$\vartheta^\circ_{\text{THEOR.Ni/L}} = 0.7974(\vartheta^\circ_{\text{EXP.PSe}}) + 31.782 \quad (2)$$

$$\vartheta^\circ_{\text{THEOR.Ir/L}} = 0.7593(\vartheta^\circ_{\text{EXP.PSe}}) + 28.023 \quad (3)$$

Quantification of electronic parameters

The electronic descriptors of the biaryl phosphines **1** – **6** and PPh_3 (**7**) were firstly determined from the ^{31}P - ^{77}Se coupling constants ($^1J_{\text{P-Se}}$) of the corresponding phospho-selenides **1a** – **7a** (Table 4). This well-established approach has been demonstrated to measure the sigma-donor character of the phosphorus center,^{15,22,24,42,44–52} governed by Bent's rule⁶³ and the Fermi-contact interactions⁶⁴ between the respective *s*-orbitals of the P and Se atoms. Through the $^1J_{\text{P-Se}}$ constants of the phospho-selenides **1a** – **7a**, it was observed that the σ -donor character of the phosphines increases in the order **3** < **6** < **7** < **2** < **5** < **4** < **1** (entries 1 – 2, Table 4). The observed electronically diametric natures of biaryl phosphacycles **1** ($^1J_{\text{P-Se}} = 673$ Hz) and **3** ($^1J_{\text{P-Se}} = 780$) is consistent with the previous prediction by Pringle.⁶¹ To our knowledge, these quantitative findings provide unprecedented electronic comparisons of phosphines derived from the Phob and Cg moieties. The observed electronic indexing of phosphines **4** – **7** employing $^1J_{\text{P-Se}}$ constants (entries 4 – 7, Table 4) is consistent with previous findings.⁴²

To quantify the overall σ -donor and π -acceptor capabilities of the phosphines **1** – **7**, the corresponding *trans*- $[\text{RhCl}(\text{CO})\text{L}_2]$ **1d** – **7d** were synthesised following literature protocols.^{17,65,66} The synthesis of *trans*- $[\text{RhCl}(\text{CO})\text{L}_2]$ **1d**, **4d**, **5d**, and **7d** proceeded efficiently with isolated yields ranging between 70 – 90%. In contrast, the synthesis of $[\text{RhCl}(\text{CO})\text{L}_2]$ **2d**, **3d**, and **6d** bearing the sterically hindered ligands ($\vartheta^\circ \geq 220$) either proceeded at diminished product yields (**3d**, 2% isolated yield), favoured the dirhodium complex (**2d**, Fig. 8), or was

unsuccessful (**6d**) after repeated attempts. Several authors have previously reported the reluctance of sterically hindered phosphines to coordinate to metal carbonyl complexes.^{37,51,67,68}

Table 4. Electronic descriptors of phosphines **1** – **7** derived from several experimental and theoretical approaches.^a

Entry	PR ₃ ^b	¹ J _{P-Se} (Hz) ^c	ν _{CO} (cm ⁻¹) ^d	ΔE (kcal/mol) ^e		V _{min} (kcal/mol) ^f
				PR ₃ Se	RhCl(CO)L ₂	
1	1	673	1949.76	-2.04	-39.70	-30.08
2	2	705	^g	0.59	-17.95	-39.56 ⁱ
3	3	780	1982.64	7.27	18.23	-28.50 ⁱ
4	4	691	1944.04	-3.12	-38.10	-33.08
5	5	697	1961.20	-3.26	-35.90	-37.22 ⁱ
6	6	735	^h	6.01	17.50	-35.96
7	7	733	1961.20	1.35	-14.73	-27.41

^aQuantification of electronic parameters of biaryl phosphacycles **1** – **3**, dialkylbiaryl phosphines **4** – **6**, and PPh₃ (**7**). Additional electron parameters included in ESI† (Table S28). ^bPhosphines. ^cExperimental ³¹P-⁷⁷Se coupling constant of phospho-selenides **1a** – **7a**. ^dExperimental C-O stretching frequency of *trans*-[RhCl(CO)L₂] **1d** – **7d** complexes (ν_{CO}, cm⁻¹). ^eComputed energy released (ΔE) in the theoretical formation of phospho-selenides **1a** – **7a** and *trans*-[RhCl(CO)L₂] **1d** – **7d** from DFT structures. ^fMolecular electrostatic potential of phosphines **1** – **7** from DFT structures, employing equation: $V(\mathbf{r}) = \sum_A^N \frac{Z_A}{|\mathbf{r} - \mathbf{R}_A|} - \int \frac{\rho(\mathbf{r}')d^3\mathbf{r}'}{|\mathbf{r} - \mathbf{r}'|}$. ^gFavoured the Rh-dimer complex. ^hUnsuccessful after repeated attempts. ⁱOverlap of the lone-pair electron density of the P and O atoms.

Moreover, Tyler and co-workers demonstrated that sterically hindered *P*-alkyl groups reduce the phosphine's ability to σ-donate by increasing its p character, a phenomenon known as back strain.³⁷ Single-crystal X-ray diffraction confirmed the molecular structures of the square planar *trans*-[RhCl(CO)L₂] **1d**, **3d**, **5d**, and **7d** (Table 5). The structure obtained of the well-known Rh-complex **7d** was reported previously by Rheingold and co-worker⁶⁹ (CSD refcode CTPRHC02) and is included here for structural comparisons.

Based on the obtained ν_{CO} (cm⁻¹) values, biaryl phosphacycle **1** (1949.76 cm⁻¹) and dialkylbiaryl phosphine **4** (1944.04 cm⁻¹) were stronger σ-donors, opposed to biaryl phosphacycles **3** (1982.64 cm⁻¹) which exhibited stronger π-accepting character (Table 4). Most notable, the shorter Rh-P (2.3205 Å) and Se-P (2.0994 Å) bond lengths of the electron-deficient bulky biaryl phosphacycles **3** when compared to the electron-rich biaryl phosphacycles, further confirms the enhanced p character of the C_g moiety. Despite the different strategies used by the two experimental approaches ¹J_{P-Se} (Hz) and ν_{CO} (cm⁻¹), a linear relationship obeying equation (4) and R² value of 0.8272 (Fig. S10, ESI†) was observed in their comparison.

$$\nu_{\text{CO}} = 0.3167(^1J_{\text{P-Se}}) + 1733.4 \quad (4)$$

To assess the experimental electronic parameterisation of phosphines **1** – **7**, the well-known computational methodologies, bond enthalpy (ΔE) and molecular electrostatic potential (MESP) were employed. The theoretical reactions of phosphines **1** – **7** with KSeCN and [RhCl(CO)₂]₂ to form the corresponding phospho-selenides and *trans*-[RhCl(CO)L₂] complexes (equation 5 and 6), respectively, allowed for the quantification of the computed energy released (ΔE). This approach which corresponds to the electron-donating strength of PR₃ has been previously employed by several authors.^{70–74}

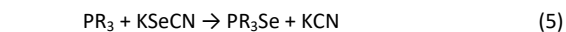
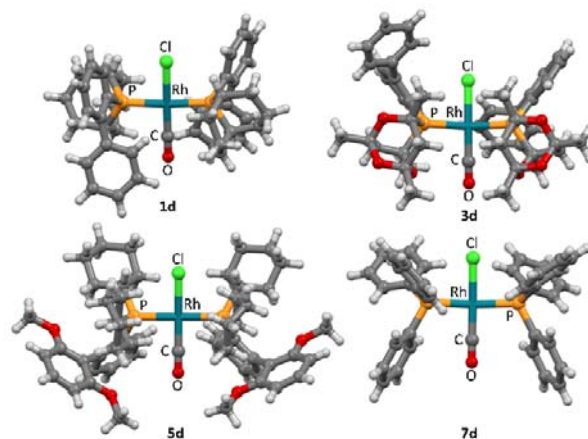


Table 5. Selected crystallographic data, refinement parameters, molecular structures, bond lengths and angles of *trans*-[RhCl(CO)L₂] **1d**, **3d**, **5d** and **7d**.^a

RhCl(CO)L ₂	1d ^b	3d ^c	5d	7d
CCDC no.	2120401	2120402	2120400	CTPRHC02 ⁶⁹
Empirical formula	C ₄₃ H ₅₀ Cl ₅ OP ₂ Rh	C ₅₁ H ₆₄ ClO ₇ P ₂ Rh	C ₅₃ H ₇₀ ClO ₅ P ₂ Rh	C ₃₇ H ₃₀ ClOP ₂ Rh
Crystal system	Orthorhombic	Triclinic	Triclinic	Monoclinic
Space group	<i>Pbca</i>	<i>P</i> -1	<i>P</i> -1	<i>P</i> 2 ₁ / <i>n</i>
a/Å	17.93190 (10)	12.1330(2)	12.08700 (10)	11.968(3)
b/Å	17.95520 (10)	12.3022(2)	14.5363(2)	24.505(7)
c/Å	26.01420 (10)	16.7869(3)	15.7989(2)	12.191(4)
α/°	90	81.1970(10)	63.5760(10)	90
β/°	90	87.7150(10)	86.7820(10)	113.27(2)
γ/°	90	72.921(2)	84.9520(10)	90
Final R indexes [I>=2σ(I)]	R ₁ = 0.0248, wR ₂ = 0.0625	R ₁ = 0.0417, wR ₂ = 0.1006	R ₁ = 0.0265, wR ₂ = 0.0685	R ₁ = 0.0370
^d Rh-P (Å)	2.3216(5)	2.3205(7)	2.3302(4)	2.300
Rh-C (Å)	1.8060(2)	1.821(3)	1.821(2)	1.820
C≡O (Å)	1.149(3)	1.144(4)	1.130(2)	1.142
^e P-Rh-CO (°)	92.36(7)	93.96(9)	89.50(6)	91.75
^e P-Rh-Cl (°)	87.644(18)	86.55(2)	91.800(15)	88.33



^aComplete crystallographic data and molecular structures can be retrieved from the ESI† (Table S6 – S7). ^bCo-crystallised with two molecules of DCM. ^cCo-crystallised with hexane. ^dAverage bond lengths or angles. The *trans*-[RhCl(CO)L₂] **1d**, **3d**, **5d** and **7d** complexes exhibited square planar geometries with P-Rh-CO and P-Rh-Cl bond angles ranging between 86.56° – 93.96°.

In general, the theoretical formations of phospho-selenides **1a**, **4a**, and **5a** were associated with the release of energy ranging from -3.26 to -2.04 kcal/mol (entries 1, 3, and 5, Table 4). In contrast, the theoretical formations of phospho-selenides **2a**, **3a**, **6a**, and **7a** were characterised by energy absorptions with magnitudes ranging from 0.59 to 7.27 kcal/mol (entries 2 – 3 and 6 – 7, Table 4). Despite the unexpectedly high energy released from the theoretical formation of phospho-selenide **5a**, the theoretical formation of phospho-selenides **1a** and **4a** are consistent with their experimental synthesis, which proceeded at 100% conversion at room temperature, opposed to the experimental synthesis of phospho-selenides **2a**, **3a**, and **5a** – **7a**, which proceeded at elevated temperatures. Similarly, the theoretical formations of $[\text{RhCl}(\text{CO})\text{L}_2]$ **1d** and **4d** complexes resulted in the highest energy released (-39.70 and -38.10 kcal/mol, respectively), opposed to the theoretical formations of $[\text{RhCl}(\text{CO})\text{L}_2]$ **3d** and **6d** (18.23 and 17.50 kcal/mol, respectively), suggesting stronger σ -donor character from biaryl phosphines **1** and **4**.

Based on the obtained theoretical bond enthalpies (ΔE) of phospho-selenides **1a** – **7a**, the electron-donating strength of the phosphines increases in the order **3** < **6** < **7** < **2** < **1** < **4** < **5**. This trend differed slightly from the one observed with the experimental $^1J_{\text{P-Se}}$ (Hz) values, but closely correlated to the one obtained with experimental ν_{CO} (cm^{-1}) (Fig. 5). The observed linear correlation between the theoretical ΔE_{PSe} and experimental ν_{CO} (cm^{-1}) follows equation (7) with an R^2 value of 0.9982.

$$\Delta E_{\text{PSe}} = 0.2740(\nu_{\text{CO}}) - 535.92 \quad (7)$$

On the other hand, the observed trend for the σ -donor character of phosphines **1** – **7** obtained from the experimental $^1J_{\text{P-Se}}$ was reproduced from the computed formation energy of $[\text{RhCl}(\text{CO})\text{L}_2]$ complexes, **3** < **6** < **7** < **2** < **5** < **4** < **1**. The observed linear correlation between the theoretical ΔE_{Rh} and experimental $^1J_{\text{P-Se}}$ (Hz) follows equation (8) with an R^2 value of 0.9731 (Figure S20, ESI†). It is worth noting that the correlation between the theoretical $\Delta E_{\text{Rh/L}}$ and experimental ν_{CO} (cm^{-1}) also follows a linear relationship with R^2 value of 0.9736 (Figure S19, ESI†).

$$\Delta E_{\text{Rh/L}} = 1.566(^1J_{\text{P-Se}}) - 3086.90 \quad (8)$$

It was observed that the theoretical bond enthalpies of phospho-selenides (ΔE_{PSe}) and *trans*- $[\text{RhCl}(\text{CO})\text{L}_2]$ complexes ($\Delta E_{\text{Rh/L}}$) were sensitive to electronic effects with the highest energy absorbed resulting from the theoretical reactions featuring the electron-deficient biaryl phosphacycle **3** ($\Delta E = 7.27$ and 18.23 kcal/mol, respectively). On the other hand, the computed formation energy of $[\text{NiCO}_3\text{L}]$ ($\Delta E_{\text{Ni/L}}$) and $[\text{IrCl}_3(\text{CO})_2\text{L}]$ ($\Delta E_{\text{Ir/L}}$) complexes were sensitive to steric effects with the highest energy absorbed resulting from the theoretical reactions featuring the most sterically hindered ($\vartheta^\circ = 228.5$) dialkylbiaryl phosphine **6** ($\Delta E = 2.33$ and 7.92 kcal/mol, Table S27).

Lastly, the electronic descriptors of phosphines **1** – **7** were quantified from their molecular electrostatic potentials (MESP) of the respective theoretical DFT B3LYP-GD3/def2-TZVPP structures using the Gaussian 09 rev E01 software⁶² and Multiwfn⁷⁵. This method provides direct quantification of the lone-pair region of PR_3 ligands and has been amply utilized by several authors.^{10,12–14,29,40,70,71} The unexpectedly large negative V_{min} values of phosphines

2, **3**, and **5** resulted from the overlap of the P lone-pair region and that of the present oxygen atoms (ESI^\ddagger).

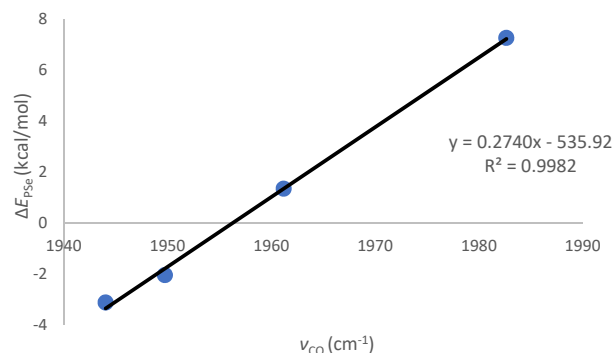


Fig. 5: Correlation between experimental ν_{CO} (cm^{-1}) of selected *trans*- $[\text{RhCl}(\text{CO})\text{L}_2]$ complexes and the computed energy released (ΔE) from the theoretical formation of selected phospho-selenides.

It was observed that the theoretical electron density around the P-donor atom increases in the order **7** < **1** < **4** < **6** from the non-oxygen containing phosphines (entries, 1, 4, 6, and 7, Table 4). The MESP theoretical quantifications provided the unprecedented electronic indexing of biaryl phosphacycle **1** comprising of the underexplored Phob moiety (Fig. 6) relative to phosphines comprising of the well-established Ph, Cy, and ^tBu moieties.^{12–14,25,70} Despite the sufficient lone-pair electron density of the theoretical structure of dialkylbiaryl phosphine **6** ($V_{\text{min}} = -35.96$ kcal/mol), its donor capabilities (determined from experimental $^1J_{\text{P-Se}}$ and theoretical ΔE) are significantly reduced due to back strain induced by the steric hindrance of the ^tBu moiety ($\vartheta^\circ = 228.5$).^{37,68} In contrast, the less hindered ($\vartheta^\circ \leq 181.3$) biaryl phosphines **1** ($V_{\text{min}} = -30.08$ kcal/mol) and **4** ($V_{\text{min}} = -33.08$ kcal/mol) demonstrated greater donor capabilities and thus ease of reactions with Se and Rh (according to experimental $^1J_{\text{P-Se}}$, ν_{CO} , and theoretical ΔE).

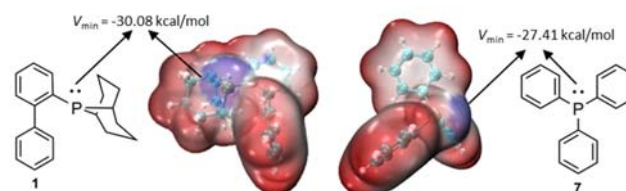


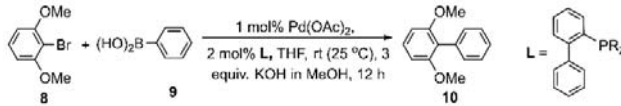
Fig. 6: The MESP isosurface of biaryl phosphacycles **1** and PPh_3 (**7**).

Structure-activity analysis

The effects of the aforementioned stereoelectronic parameters were first investigated in the Suzuki-Miyaura coupling of aryl bromide **8** and boronic acid **9**, as shown in Table 6. Efficient synthesis of biaryl product **10** (GC yield $\geq 94\%$) was observed with the electron rich ($^1J_{\text{P-Se}} \leq 691$ Hz) and less hindered ($\vartheta \leq 181.3^\circ$) biaryl phosphines **1** and **4** (Table 6, entries 1 and 3, respectively). Catalysts derived from the excessively hindered ($\vartheta \geq 222.0^\circ$) biaryl phosphines **2** and **6** afforded lower yields (GC yield $\leq 10\%$) of the desired biaryl product **10** (entries 2 and 4, respectively).

Most notably, it was observed that this coupling reaction (Table 6) as well as others that we have previously reported^{43–45} are more sensitive to the ligand's steric bulk (Fig. 7).

Table 6: Effects of stereoelectronic parameters in the Suzuki-Miyaura coupling of aryl bromide **8** and boronic acid **9**.^a



Entry	R ^b	Ligand	Cone angle (θ°) ^c	¹ J _{P,Se} (Hz) ^d	Yield (%) ^e
1	Phob[3.3.1]	1	178.5	673	97
2	Cg	3	222.0	780	10
3	Cy	4	181.3	691	94
4	^t Bu	6	228.5	735	7

^aReaction conditions⁴³: ArBr (1 equiv.), ArB(OH)₂ (1.5 equiv.), 2 M KOH in MeOH (3 equiv.), Pd(OAc)₂ (1 mol%), L (2 mol%), THF, Ar, 12 h, rt (25 °C). GC yields from an average of two runs with <5% deviation. ^bPhob[3.3.1] = phosphabicyclo[3.3.1]nonane, and Cg = 1,3,5,7-tetramethyl-2,4,6-trioxo-8-phosphaadamantane. ^cExact cone angle (°) obtained from crystallographic phospho-selenides. ^dExperimental ³¹P-⁷⁷Se coupling constant of PR₃Se.

In general, these findings suggest that coupling of *meta*- and *para*-substituted aryl bromides as well as chloro-heterocycles proceed efficiently in the presence of ligands with cone angles ranging from 178.5° to 222.0°. Those with cone angles ranging from 178.5° to 181.3° are efficient for coupling of *ortho*-substituted substrates (Figure 6). Despite being electron-deficient, the sterically hindered biaryl phosphine **3** (θ = 222.0°) was effective in coupling of heterocyclic, and *meta*- and *para*-substituted substrates.

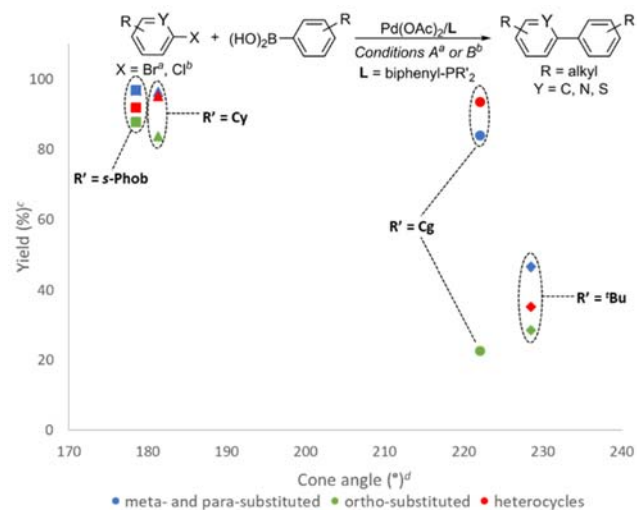


Fig. 7: A structure-activity analysis of biaryl phosphines **1** (square), **3** (triangle), **4** (circle), and **6** (diamond) in selected Suzuki-Miyaura cross-coupling reactions of *meta*- and *para*-substituted aryl bromides (blue), *ortho*-substituted aryl bromides and boronic acids (green) as well as heterocyclic chlorides (red).⁴³ Reaction conditions A: ^aArBr (1 equiv.), ArB(OH)₂ (1.5 equiv.), 2 M KOH in MeOH (3 equiv.), Pd(OAc)₂ (2 mol%), L (5 mol%), THF, Ar, 12 h, rt (25 °C). Reaction conditions B: ^aArCl (1 equiv.), ArB(OH)₂ (1.5 equiv.), K₃PO₄ (2 equiv.), Pd(OAc)₂ (1 mol%), L (2 mol%), toluene, 100 °C, 12 h, Ar. ^eAverage GC yields from an average of two runs with <5% deviation. ^cExact cone angle (°) obtained from crystallographic phospho-selenides. The selected examples are included in the ESI† (Table S29).

Conclusions

The diverse steric parameterisation study first provided a detailed steric index of the recently developed biaryl phosphacycles **1** – **3** as well as better insights into the applicability of phospho-selenides for the determination of steric parameters (% V_{Bur}, θ°, and Ω°). Secondly, we observed a decrease in the magnitudes of the steric parameters as we move from the non-metal phospho-selenides to the more congested tetrahedral [NiCO₃L] and octahedral [IrCl₃(CO)₂L] structures. The FindConeAngle package provided steric parameters (θ°) with better correlations (R² = 0.9790 – 0.9944) when compared to Solid-G (Ω°) and SambVca (% V_{Bur}). Our successful attempts toward electronic parameterisation of biaryl phosphacycles **1** – **3** primarily through ³¹P-⁷⁷Se coupling constants demonstrated comparable electronic parameters of biaryl phosphacycles **1** – **2** and dialkylbiaryl phosphines **4** – **5**, derived from phobane and cyclohexyl moieties, respectively. The electron-deficient character of biaryl phosphacycles **3** comprising of the phosphatrioxa-adamantane moiety was consistently observed throughout the electronic parameterisation studies. The poor metal-coordination ability of the sterically hindered biaryl phosphines **2**, **3**, and **6** is believed to be a result of the sterically induced reduction of the P-basicity. Our successful attempts to establish structure-activity relationships revealed that fine-tuned ligand steric bulk is more pivotal for efficient catalyst systems for Suzuki-Miyaura cross-coupling reactions of a variety of substrates. Steric and electronic studies on a variety of conformers for the described phosphines are currently in progress and will be disclosed in due course.

Experimental

General

All chemicals and solvents were purchased from Sigma-Aldrich. Transformations that involve phosphorus derivatives were unless otherwise stated. NMR-spectroscopy was performed in CDCl₃ solutions using Bruker Ultrashield 400 MHz magnet, an Avance III 400 MHz Console or 500 MHz magnet coupled to an Avance III HD 500 MHz Console. IR data was obtained from a SHIMADZU IR Affinity-1S, with the characteristic peaks reported in wavenumber (cm⁻¹). High-resolution mass spectral analyses were performed on a Waters® Synapt G2 high-definition mass spectrometer (HDMS) that consists of a Waters Acquity Ultra Performance Liquid Chromatography (UPLC®) system hyphenated to a quadrupole-time-of-flight (QTOF) instrument. The synthesis and full characterisation of the *P*-bridged biaryl phosphacycles **1** – **3** is described in our previous work.⁴³ Dialkylbiaryl phosphines **4** – **6** and PPh₃ (**7**) were purchased from Sigma-Aldrich and used without any purification. The provided literature reports comprise of the synthesis and characterisation of **4**⁷⁶, **5**⁷⁷, and **6**⁷⁶.

Crystallography

Single crystal X-ray diffraction was conducted on a Rigaku XtaLAB Synergy R diffractometer, with a rotating-anode X-ray source and a HyPix CCD detector. Data reduction and absorption were carried out using the CrysalisPro (version 1.171.40.23a) software package.⁷⁸ All X-ray diffraction measurements were performed at 150 K, using an

Oxford Cryogenics Cryostat. All structures were solved by direct methods with SHELXS and SHELXL softwares^{79,80} using the OLEX2⁸¹ interface. All H atoms were placed in geometrically idealised positions and constrained to ride on their parent atoms. For data collection and refinement parameters, see (Tables S2, S4, S6). The X-ray structures have been deposited at the Cambridge Crystallographic Data Centre (CCDC), with deposition numbers CCDC: phospho-selenides **1a** (2051977), **2a** (2051921), **3a** (2051993), **4a** (2051992), **5a** (2052006), and **6a** (2051994), *trans*-[RhCl(CO)L₂] **1d** (2120401), **3d** (2120402), **5d** (2120400) and the dirhodium **2d** (2120403). The data can be obtained free of charge from The Cambridge Crystallographic Data Centre via www.ccdc.cam.ac.uk/data_request/cif.

Computational methods and programs

All computational models were built using the Gaussview 5.0 molecular builder and optimized using the Gaussian 09 rev E01 software installed on the Lengau Cluster of the Centre for High Performance Computing (CHPC), South Africa.⁶² Steric descriptors were quantified using the packages; Solid-G²⁴, SambVca⁵⁸, and FindConeAngle³² implemented in Mathematica⁸². For all quantifications, the default settings were employed. Molecular electrostatic potentials (MESP) were calculated using the Multiwfn.⁷⁵ The corresponding MESP isosurface were accessed from the Visual molecular dynamics (VMD) program.⁸³

Synthesis of phospho-selenides

A slightly modified methodology reported by Muller was adopted.⁵⁴ Tertiary phosphines (20 mg) were dissolved in degassed and anhydrous DCM (0.25 cm³), this was added dropwise to equimolar amounts of KSeCN dissolved in degassed and dry MeOH (0.25 cm³) in a Schlenk tube under argon, i.e 1 equiv 3° phosphine: 1 equiv. KSeCN. The reaction mixture was allowed to stir at room-temperature (25 °C) under argon for 12 h. This method was applicable for the strongly electron rich ligands **1** and **4**. For phosphines **2**, **5** and **7**, the reactions were conducted at 100 °C (12 h) to achieve full conversion of the 3° phosphines to the corresponding phospho-selenides. An excess of 20 equiv. KSeCN was used for full conversion of **6** to **6a** (reflux in toluene, 24 h), **3** to **3a** (reflux in H₂O/acetonitrile, 48 h). Similar conditions were adopted by Sigman⁴² to achieve full conversions of sterically hindered phosphines to the corresponding phospho-selenides. The reactions were monitored by ³¹P-NMR, upon completion the reaction mixtures were recrystallised from DCM/MeOH (1:1) at room temperature (25 °C) to give the desired products.

[[1,1'-biphenyl]-2-yl]-9-phosphabicyclo[3.3.1]nonane-9-selenide (compound 1a), 97%. ³¹P NMR (202 MHz, CDCl₃) δ = 29.06 (¹J_{P-Se} = 673 Hz). ¹H NMR (400 MHz, CDCl₃) δ = 8.36 (bs, 1H), 7.67 – 7.60 (m, 1H), 7.50 – 7.26 (m, 7H), 3.04 (bs, 1H), 2.65 (bs, 1H), 2.52 (d, J = 15.9 Hz, 1H), 2.01 – 1.80 (m, 5H), 1.69 – 1.50 (m, 4H), 1.38 – 1.27 (m, 1H), 1.06 (d, J = 16.7 Hz, 1H). ¹³C NMR (126 MHz, CDCl₃) δ = 144.73 (d, J_{C-P} = 6.5 Hz), 140.65 (d, J_{C-P} = 2.9 Hz), 132.38 (d, J_{C-P} = 9.2 Hz), 130.57 (d, J_{C-P} = 2.8 Hz), 130.05 (d, J_{C-P} = 9.5 Hz), 130.31 – 129.68 (m), 128.19 (s), 127.77 (d, J_{C-P} = 11.3 Hz), 31.92 (d, J_{C-P} = 37.8 Hz), 29.89 (d, J_{C-P} =

35.4 Hz), 28.11 (d, J_{C-P} = 3.8 Hz), 27.78 (d, J_{C-P} = 4.2 Hz), 27.08 (s), 26.46 (s), 20.88 (d, J_{C-P} = 5.5 Hz), 20.77 (d, J_{C-P} = 5.4 Hz).

(2',6'-dimethoxy-[1,1'-biphenyl]-2-yl)-9-

phosphabicyclo[3.3.1]nonane-9-selenide (compound 2a), 95%. ³¹P NMR (202 MHz, CDCl₃) δ = 31.11 (¹J_{P-Se} = 705 Hz). ¹H NMR (500 MHz, CDCl₃) δ = 7.68 (dd, J = 12.9, 7.4 Hz, 1H), 7.44 (p, J = 7.2 Hz, 2H), 7.29 (t, J = 8.4 Hz, 1H), 7.22 (dd, J = 7.8, 3.3 Hz, 1H), 6.53 (d, J = 8.3 Hz, 2H), 3.70 (s, 6H), 3.12 (s, 1H), 2.56 (d, J = 93.9 Hz, 2H), 2.14 (d, J = 6.2 Hz, 2H), 1.93 – 1.82 (m, 3H), 1.69 – 1.50 (m, 3H), 1.41 – 1.35 (m, 1H), 1.21 (d, J = 18.4 Hz, 2H). ¹³C NMR (126 MHz, CDCl₃) δ = 158.39 (s), 137.25 (d, J_{C-P} = 6.5 Hz), 133.63 (d, J_{C-P} = 9.8 Hz), 131.43 (s), 130.90 (s), 130.48 – 129.96 (m), 127.69 (d, J_{C-P} = 11.5 Hz), 116.87 (d, J_{C-P} = 2.9 Hz), 103.37 (s), 55.34 (s), 53.40 (s), 31.64 (s), 29.70 (s), 27.40 (s), 21.05 (d, J_{C-P} = 5.8 Hz), 20.77 (d, J_{C-P} = 6.0 Hz).

[[1,1'-biphenyl]-2-yl]-1,3,5,7-tetramethyl-2,4,6-trioxa-8-

phosphaadamantane-8-selenide (compound 3a), 90%. ³¹P NMR (202 MHz, CDCl₃) δ = 22.99 (¹J_{P-Se} = 780 Hz). ¹H NMR (500 MHz, CDCl₃) δ = 8.72 – 8.65 (m, 1H), 7.50 (t, J = 7.4 Hz, 1H), 7.42 (t, J = 7.6 Hz, 1H), 7.35 – 7.22 (m, 6H), 3.47 (dd, J = 13.6, 3.8 Hz, 1H), 2.27 (d, J = 14.0 Hz, 1H), 1.95 (dd, J = 22.4, 14.0 Hz, 1H), 1.62 (dd, J = 25.6, 13.6 Hz, 1H), 1.55 (d, J = 14.2 Hz, 3H), 1.46 (s, 3H), 1.37 (s, 3H), 1.32 (d, J = 15.0 Hz, 3H). ¹³C NMR (126 MHz, CDCl₃) δ = 150.94 (d, J_{C-P} = 9.4 Hz), 140.91 (d, J_{C-P} = 3.4 Hz), 134.89 (d, J_{C-P} = 10.1 Hz), 132.40 (d, J_{C-P} = 6.1 Hz), 131.10 (d, J_{C-P} = 2.9 Hz), 130.91 (s), 127.46 (s), 126.84 – 126.45 (m), 124.29 (s), 123.89 (s), 96.58 (s), 96.15 (d, J_{C-P} = 1.3 Hz), 78.69 (s), 78.40 (s), 73.34 (s), 73.03 (s), 40.78 (d, J_{C-P} = 6.0 Hz), 39.38 (d, J_{C-P} = 4.3 Hz), 27.68 (s), 27.25 (s), 24.82 (d, J_{C-P} = 3.3 Hz), 22.07 (d, J_{C-P} = 2.1 Hz).

[1,1'-biphenyl]-2-ylidicyclohexylphosphine selenide (compound 4a)

, 98%.⁴² ³¹P NMR (162 MHz, CDCl₃) δ = 68.77. (¹J_{P-Se} = 692 Hz). ¹H NMR (500 MHz, CDCl₃) δ = 8.78 (dd, J = 16.1, 7.7 Hz, 1H), 7.48 (dd, J = 21.6, 7.0 Hz, 5H), 7.23 (d, J = 7.2 Hz, 2H), 7.12 (s, 1H), 1.66 (d, J = 9.7 Hz, 10H), 1.55 (s, 3H), 1.31 (d, J = 8.0 Hz, 2H), 1.16 – 1.02 (m, 7H). ¹³C NMR (126 MHz, CDCl₃) δ = 143.06 (d, J_{C-P} = 5.8 Hz), 142.07 (s), 139.16 (d, J_{C-P} = 12.8 Hz), 131.34 (d, J_{C-P} = 8.8 Hz), 130.57 (d, J_{C-P} = 2.8 Hz), 129.02 (s), 128.32 (s), 128.04 (s), 127.60 (d, J_{C-P} = 12.2 Hz), 125.93 (s), 125.49 (s), 38.66 (s), 38.33 (s), 29.35 (d, J_{C-P} = 2.1 Hz), 27.03 (d, J_{C-P} = 1.8 Hz), 26.12 (t, J_{C-P,Se} = 13.6 Hz), 25.41 (s).

Dicyclohexyl(2',6'-dimethoxy-[1,1'-biphenyl]-2-yl)phosphine

selenide (compound 5a) 94%.⁴² ³¹P NMR (202 MHz, CDCl₃) δ = 67.90 (¹J_{P-Se} = 697 Hz). ¹H NMR (500 MHz, CDCl₃) δ = 8.74 – 8.67 (m, 1H), 7.43 (dd, J = 4.3, 2.7 Hz, 2H), 7.38 (t, J = 8.4 Hz, 1H), 7.02 (dd, J = 8.4, 4.3 Hz, 1H), 6.64 (d, J = 8.4 Hz, 2H), 3.67 (s, 6H), 1.88 (dd, J = 9.1, 5.8 Hz, 2H), 1.72 – 1.58 (m, 8H), 1.52 (d, J = 12.5 Hz, 2H), 1.42 – 1.31 (m, 2H), 1.28 (s, 2H), 1.14 – 0.99 (m, 6H). ¹³C NMR (126 MHz, CDCl₃) δ = 158.11 (s), 138.55 (d, J_{C-P} = 12.4 Hz), 136.76 (d, J_{C-P} = 5.3 Hz), 132.86 (d, J_{C-P} = 8.9 Hz), 130.53 (d, J_{C-P} = 2.8 Hz), 129.79 (s), 127.82 (s), 127.37 (s), 126.78 (d, J_{C-P} = 12.1 Hz), 119.23 (s), 103.95 (s), 55.85 (s), 38.00 (s), 37.68 (s), 29.69 (s), 28.74 (d, J_{C-P} = 2.1 Hz), 27.31 (d, J_{C-P} = 1.9 Hz), 26.39 (dd, J_{C-P} = 14.0, 5.9 Hz), 25.54 (s).

[1,1'-biphenyl]-2-ylid-tert-butylphosphine selenide (compound 6a), 91%. ^{31}P NMR (202 MHz, CDCl_3) δ = 71.17 ($J_{\text{P-Se}}$ = 735 Hz). ^1H NMR (400 MHz, CDCl_3) δ = 8.15 – 8.05 (m, 1H), 7.49 – 7.42 (m, 2H), 7.38 – 7.29 (m, 5H), 7.16 – 7.09 (m, 1H), 1.59 (s, 5H), 1.27 (d, J = 3.0 Hz, 6H), 1.21 (s, 4H), 1.13 (s, 3H). ^{13}C NMR (101 MHz, CDCl_3) δ = 151.24 (d, $J_{\text{C-P}}$ = 32.6 Hz), 143.81 (d, $J_{\text{C-P}}$ = 7.1 Hz), 135.59 (d, $J_{\text{C-P}}$ = 27.9 Hz), 135.37 (d, $J_{\text{C-P}}$ = 3.3 Hz), 130.65 – 130.54 (m, $J_{\text{C-P,Se}}$), 128.37, 127.14, 126.42, 125.76, 32.74 (d, $J_{\text{C-P}}$ = 25.0 Hz), 30.75 (d, $J_{\text{C-P}}$ = 15.4 Hz).

Synthesis of *trans*-[RhCl(CO)L₂]

Literature protocols were adopted in the synthesis of *trans*-[RhCl(CO)L₂].^{17,65,66} [Rh₂Cl₂(CO)₄] (2.0 mg) dissolved in degassed and anhydrous acetone (0.1 cm³) was treated with a solution of tertiary phosphines (4.0 equiv.) in degassed and anhydrous acetone (0.1 cm³). The reactions were allowed to run for 12 h at 30 °C. The reaction mixture was filtered, concentrated and recrystallized from DCM:hexane (1:2). This method was applicable for the reactions featuring the less hindered phosphines **1**, **4**, **5**, and **7**.

[RhCl(CO)(1)₂] (complex 1d), 91%. IR $\nu_{\text{max}}(\text{film})/\text{cm}^{-1}$: 1949.76s (C-O). ^{31}P NMR (202 MHz, CDCl_3) δ = 14.21 (d, $J_{\text{Rh-P}}$ = 119.4 Hz). ^1H NMR (500 MHz, CDCl_3) δ = 8.34 – 7.96 (m, 2H), 7.88 (bs, 2H), 7.48 – 7.23 (m, 12H), 7.17 (d, J = 6.7 Hz, 2H), 3.30 – 2.42 (m, 7H), 2.04 – 1.60 (m, 16H), 1.30 – 1.06 (m, 5H). ^{13}C NMR (126 MHz, CDCl_3) δ = 144.93, 142.04, 134.01, 131.01, 128.62, 128.18, 128.10, 127.55, 126.92, 31.96, 31.51, 30.59, 29.44, 29.12, 27.67, 27.47, 26.20, 26.10, 25.21, 24.94, 21.99, 21.45. HR-ESI-MS: Calculated m/z = 719.2079 [M - Cl]⁺, Found m/z = 719.2183 [M - Cl]⁺.

[RhCl(CO)(4)₂] (complex 4d), 94%. IR $\nu_{\text{max}}(\text{film})/\text{cm}^{-1}$: 1944.04s (C-O). Neither the ^{31}P NMR, ^1H NMR, and ^{13}C NMR spectra could be recorded for **4d** as it was insoluble in a variety of deuterated solvents. Unfortunately, several attempts to recrystallise **4d** were unsuccessful. HR-ESI-MS: Calculated m/z = 831.3331 [M - Cl]⁺, Found m/z = 831.3416 [M - Cl]⁺.

[RhCl(CO)(5)₂] (complex 5d), 88%. IR $\nu_{\text{max}}(\text{film})/\text{cm}^{-1}$: 1961.20s (C-O). ^{31}P NMR (202 MHz, CDCl_3) δ = 49.73 (d, J = 124.3 Hz). ^1H NMR (500 MHz, CDCl_3) δ = 8.34 (d, J = 3.4 Hz, 1H), 7.36 – 7.28 (m, 3H), 6.93 (d, J = 3.3 Hz, 1H), 6.57 (d, J = 8.4 Hz, 2H), 3.60 (s, 6H), 2.17 (d, J = 20.8 Hz, 2H), 1.93 (d, J = 11.6 Hz, 2H), 1.62 (dd, J = 39.0, 13.4 Hz, 8H), 1.39 – 1.32 (m, 2H), 1.16 – 1.00 (m, 5H), 0.97 – 0.85 (m, 3H). ^{13}C NMR (126 MHz, CDCl_3) δ = 157.93, 139.60, 138.37, 132.23, 128.96, 128.70, 124.94, 124.89, 124.84, 119.79, 103.37, 55.00, 33.67, 33.59, 33.51, 31.58, 30.64, 29.17, 27.46, 27.41, 27.36, 27.23, 27.12, 26.44, 22.65. HR-ESI-MS: Calculated m/z = 951.3754 [M - Cl]⁺, Found m/z = 951.3817 [M - Cl]⁺.

[RhCl(CO)(5)₂] (complex 7d)⁶⁹, 90%. IR $\nu_{\text{max}}(\text{film})/\text{cm}^{-1}$: 1961.20s (C-O). ^{31}P NMR (202 MHz, CDCl_3) δ = 28.99 (d, $J_{\text{Rh-P}}$ = 127.0 Hz). ^1H NMR (500 MHz, CDCl_3) δ = 7.74 – 7.68 (m, 12H), 7.41 – 7.33 (m, 18H). ^{13}C NMR (101 MHz, CDCl_3) δ = 134.74 (t, J = 6.4 Hz), 132.96 (t, J = 20.2), 130.10, 128.13 (t, J = 5.0 Hz). HR-ESI-MS: Calculated m/z = 655.0827 [M - Cl]⁺, Found m/z = 655.0807 [M - Cl]⁺.

Reactions with biaryl phosphacycle **2** conducted at 30 – 110 °C (acetone, DCM, toluene) for 12 – 48 h consistently led to the chloride

bridged dirhodium dimer (Fig. 8). Further treatment of the successfully isolated dirhodium dimer with biaryl phosphacycles **2** (2 – 4 equiv.) was unsuccessful. HR-ESI-MS: Calculated m/z = 839.2502 [M - RhCl₂CO]⁺, Found m/z = 839.2570 [M - RhCl₂CO]⁺.

Selected crystallographic data: C₄₈H₅₈Cl₆O₆P₂Rh₂, 1211.40 g/mol, 150.00(10) K, Monoclinic, P_{21}/c , a = 14.84410(10) Å, b = 16.21440(10) Å, c = 21.0762(2) Å, α = 90°, β = 100.1220(10)°, γ = 90°, Volume = 4993.84(7) Å³, Z = 4, and final R indexes [$I > 2\sigma(I)$]: R_1 = 0.0375, wR_2 = 0.0944.

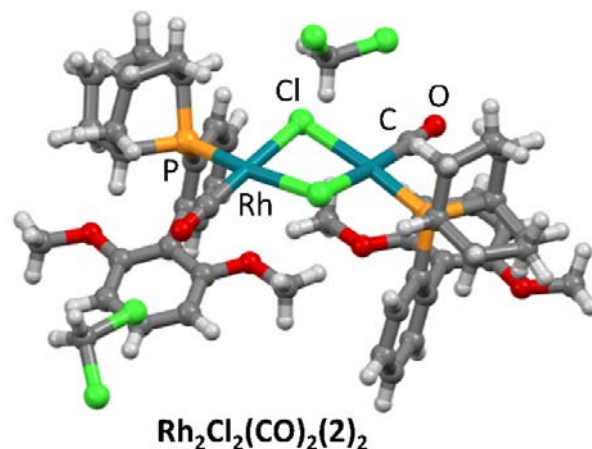


Fig. 8: Molecular structure (50% thermal ellipsoid probability) of the dirhodium dimer of phosphine **5**, containing two co-crystallised DCM molecules.

Reactions with biaryl phosphacycle **3** conducted at 60 – 110 °C (acetone and toluene) for 12 – 48 h consistently led to not more than 2% conversion of biaryl phosphacycle **3** to the desired product, based on ^{31}P -NMR analysis. ^{31}P NMR (202 MHz, CD_2Cl_2) δ = 39.78 (d, J = 149.5 Hz).

Reactions with dialkylbiaryl phosphine **6** conducted at 60 – 110 °C (acetone and toluene) for 12 – 48 h consistently led to the recovery of the unreacted phosphine.

Conflicts of interest

There are no conflicts to declare.

Acknowledgements

We are grateful for financial support from Research Centre for Synthesis and Catalysis (University of Johannesburg) and Sasol (Pty) Ltd. The authors acknowledge the Centre for High Performance Computing (CHPC), South Africa for providing computational resources to this research project.

Notes and references

- 1 A. De Meijere and F. Diederich, *Metal-Catalyzed Cross-Coupling Reactions*, Wiley-VCH, Weinheim, 2014. **Chp. 1–2**, 1–104.
- 2 P. G. Jessop, F. Joó and C. C. Tai, *Coord. Chem. Rev.*, 2004, **248**, 2425–2442.
- 3 R. Franke, D. Selent and A. Börner, *Chem. Rev.*, 2012, **112**, 5675–5732.
- 4 S. T. Gadge and B. M. Bhanage, *RSC Adv.*, 2014, **4**, 10367–10389.
- 5 G. Cavinato and L. Toniolo, *Molecules*, 2014, **19**, 15116–15161.
- 6 C. K. Chu, T. P. Lin, H. Shao, A. L. Liberman-Martin, P. Liu and R. H. Grubbs, *J. Am. Chem. Soc.*, 2018, **140**, 5634–5643.
- 7 W. L. McClennan, S. A. Ruffh, J. A. M. Lummiss and D. E. Fogg, *J. Am. Chem. Soc.*, 2016, **138**, 14668–14677.
- 8 A. Behr, *Homogeneous Catalysis*, Wiley-VCH Verlag GmbH & Co. KGaA, Weinheim, 2012. **Chp. 5**, 236–261.
- 9 S. Bhaduri and D. Mukesh, *Homogeneous Catalysis: Mechanisms and Industrial Applications*, John Wiley & Sons, Inc., New Jersey, 2014. **Chp. 6**, 167–197.
- 10 P. W. N. M. Kamer, P. C. J.; van Leeuwen, *Phosphorus(III) Ligands in Homogenous Catalysis*, John Wiley & Sons, Ltd., United Kingdom, 2012. **Chp. 1–3**, 1–123.
- 11 V. Iaroshenko, *Organophosphorus Chemistry*, Wiley-VCH Verlag GmbH & Co., Germany, 2019. **Chp. 1**, 1 - 49.
- 12 D. J. Durand and N. Fey, *Chem. Rev.*, 2019, **119**, 6561–6594.
- 13 N. Fey, *J. Chem. Soc., Dalton. Trans.*, 2010, **39**, 296–310.
- 14 N. Fey, A. G. Orpen and J. N. Harvey, *Coord. Chem. Rev.*, 2009, **253**, 704–722.
- 15 D. J. M. Snelders, G. Van Koten and R. J. M. Klein Gebbink, *Chem. A Eur. J.*, 2011, **17**, 42–57.
- 16 C. A. Tolman, *Chem. Rev.*, 1977, **77**, 313–348.
- 17 C. A. Tolman, *J. Am. Chem. Soc.*, 1970, **92**, 2953–2956.
- 18 M. Huser, M. T. Youinou and J. A. Osborn, *Angew. Chemie Int. Ed.*, 1989, **28**, 1386–1388.
- 19 J. Slanina, P. C. M. Frintrop, J. F. Mansveld and B. Griepink, *Mikrochim. Acta*, 1970, **58**, 52–57.
- 20 S. Joerg, R. S. Drago and J. Sales, *Organometallics*, 1998, **17**, 589–599.
- 21 D. W. Allen and B. F. Taylor, *J. Chem. Soc., Dalt. Trans.*, 1982, 51–54.
- 22 Z. Domínguez, J. Hernández, L. Silva-Gutiérrez, M. Salas-Reyes, M. Sánchez and G. Merino, *Phosphorus, Sulfur Silicon Relat. Elem.*, 2010, **185**, 772–784.
- 23 B. W. Tattershall and E. L. Sandham, *J. Chem. Soc. Dalt. Trans.*, 2001, 1834–1840.
- 24 I. A. Guzei and M. Wendt, *J. Chem. Soc. Dalt. Trans.*, 2006, 3991–3999.
- 25 N. Fey, A. C. Tsipis, S. E. Harris, J. N. Harvey, A. G. Orpen and R. A. Mansson, *Chem. Eur. J.*, 2005, **12**, 291–302.
- 26 J. Jover, N. Fey, J. N. Harvey, G. C. Lloyd-Jones, A. G. Orpen, G. J. J. Owen-Smith, P. Murray, D. R. J. Hose, R. Osborne and M. Purdie, *Organometallics*, 2012, **31**, 5302–5306.
- 27 B. J. Dunne, R. B. Morris and A. G. Orpen, *J. Chem. Soc. Dalt. Trans.*, 1991, 653–661.
- 28 K. D. Cooney, T. R. Cundari, N. W. Hoffman, K. A. Pittard, M. D. Temple and Y. Zhao, *J. Am. Chem. Soc.*, 2003, **125**, 4318–4324.
- 29 C. H. Suresh, N. Koga and S. R. Gadre, *Organometallics*, 2000, 3008–3015.
- 30 A. V. Brethomé, S. P. Fletcher and R. S. Paton, *ACS Catal.*, 2019, **9**, 2313–2323. Rerences cited therein.
- 31 A. C. Hillier, W. J. Sommer, B. S. Yong, J. L. Petersen, L. Cavallo and S. P. Nolan, *Organometallics*, 2003, **22**, 4322–4326.
- 32 J. A. Bilbrey, A. H. Kazez, J. Locklin and W. D. Allen, *J. Comput. Chem.*, 2013, **34**, 1189–1197.
- 33 J. Jover and J. Cirera, *J. Chem. Soc., Dalton. Trans.*, 2019, **48**, 15036–15048.
- 34 J. Ponce-De-León, R. Infante, M. Pérez-Iglesias and P. Espinet, *Inorg. Chem.*, 2020, **59**, 16599–16610.
- 35 P. Rotering, L. F. B. Wilm, J. A. Werra and F. Dielmann, *Chem. Eur. J.*, 2020, **26**, 406–411.
- 36 S. D. Laffoon, V. S. Chan, M. G. Fickes, B. Kotecki, A. R. Ickes, J. Henle, J. G. Napolitano, T. S. Franczyk, T. B. Dunn, D. M. Barnes, A. R. Haight, R. F. Henry and S. Shekhar, *ACS Catal.*, 2019, **9**, 11691–11708.
- 37 J. K. Alexander, L. N. Zakharov and D. R. Tyler, *Inorg. Chem.*, 2016, **55**, 3079–3090.
- 38 Y. Zhao, H. van Nguyen, L. Male, P. Craven, B. R. Buckley and J. S. Fossey, *Organometallics*, 2018, **37**, 4224–4241.
- 39 T. Shin, H. Kim, S. Kim, A. Lee, M. S. Seo, J. Choi, H. Kim and H. Kim, *Org. Lett.*, 2019, **21**, 5789–5792.
- 40 L. Julian, R. M. Gauld, K. Feichtner, I. Rodstein, J. Zur, J. Handelmann, C. Schwarz and V. H. Gessner, *Organometallics*, 2021, **40**, 2888–2900.
- 41 P. Saxena, J. M. Thomas, C. Sivasankar and N. Thirupathi, *New J. Chem.*, 2019, **43**, 2307–2327.
- 42 Z. L. Niemeyer, A. Milo, D. P. Hickey and M. S. Sigman, *Nat. Chem.*, 2016, **8**, 610–617, and references therein.
- 43 J. L. Lamola, P. T. Moshapo, C. W. Holzapfel and M. C. Maumela, *RSC Adv.*, 2021, **11**, 26883–26891.
- 44 J. L. Lamola, P. T. Moshapo, C. W. Holzapfel and M. Christopher Maumela, *Tetrahedron Lett.*, 2021, **88**, 153572.
- 45 J. L. Lamola, P. T. Moshapo, C. W. Holzapfel and M. C. Maumela, *Phosphorus. Sulfur. Silicon Relat. Elem.*, 2021, doi: <https://doi.org/10.1080/10426507.2021.2012178> (recently accepted).
- 46 R. J. K. Snelders, D. J., van der Burg, C., Lutz, M., Spek, A. L., van Koten, G., & Gebbink, *ChemCatChem*, 2010, **2**, 1425–1437. References cited therein.
- 47 E. Genin, R. Amengual, V. Michelet, M. Savignac, A. Jutand, L. Neuville and J. P. Genêt, *Adv. Synth. Catal.*, 2004, **346**, 1733–1741.
- 48 P. N. Bungu and S. Otto, *J. Organomet. Chem.*, 2007, **692**, 3370–3379.
- 49 S. Konishi, T. Iwai and M. Sawamura, *Organometallics*, 2018, **37**, 1876–1883.
- 50 N. Biricik, C. Kayan, B. Gümgüm, Z. Fei, R. Scopelliti, P. J. Dyson, N. Gürbüz and I. Özdemir, *Inorganica Chim. Acta*, 2010, **363**, 1039–1047.
- 51 M. L. Clarke, G. L. Holliday, A. M. Z. Slawin and J. D. Woollins, *J. Chem. Soc., Dalt. Trans.*, 2002, 1093–1103.

- 52 C. Kayan, N. Biricik and M. Aydemir, *Transit. Met. Chem.*, 2011, **36**, 513–520.
- 53 See Table S1 for a summary of previously reported systems in quantification of steric parameters of biaryl phosphines $PR_2(\text{biaryl})$.
- 54 A. Muller, *Acta Crystallogr.*, 2011, **E67**, o45-S9.
- 55 J. H. Downing, J. Roure, K. Heslop, M. F. Haddow, J. Hopewell, M. Lusi, H. Phetmung, A. G. Orpen, P. G. Pringle, R. I. Pugh and D. Zambrano-Williams, *Organometallics*, 2008, **27**, 3216–3224.
- 56 P. W. Codding and K. A. Kerr, *Acta Crystallogr.*, 1979, **B35**, 1261–1263.
- 57 M. J. Ten Hoor, *J. Chem. Educ.*, 2002, **79**, 956–957.
- 58 A. Poater, B. Cosenza, A. Correa, S. Giudice, F. Ragone, V. Scarano and L. Cavallo, *Eur. J. Inorg. Chem.*, 2009, 1759–1766.
- 59 H. Clavier and S. P. Nolan, *Chem. Commun.*, 2010, **46**, 841–861.
- 60 J. L. Lamola, J. C. Shilubana, L. Ngodwana, B. Vatsha, A. S. Adeyinka, M. C. Maumela, C. W. Holzapfel and E. M. Mmutlane, *Eur. J. Inorg. Chem.*, 2021, 2578–2582.
- 61 D. L. Dodds, J. Floure, M. Garland, M. F. Haddow, T. R. Leonard, C. L. McMullin, A. G. Orpen and P. G. Pringle, *J. Chem. Soc., Dalton. Trans.*, 2011, **40**, 7137–7146.
- 62 M. J. Frisch, G. W. Trucks, H. B. Schlegel, G. E. Scuseria, M. A. Robb, J. R. Cheeseman, G. Scalmani, V. Barone, B. Mennucci, G. A. Petersson, H. Nakatsuji, M. Caricato, X. Li, H. P. Hratchian, A. F. Izmaylov, J. Bloino, G. Zheng, J. L. Sonnenberg, M. Hada, M. Ehara, K. Toyota, R. Fukuda, J. Hasegawa, M. Ishida, T. Nakajima, Y. Honda, O. Kitao, H. Nakai, T. Vreven, J. A. Montgomery, J. E. Peralta, F. Ogliaro, M. Bearpark, J. J. Heyd, E. Brothers, K. N. Kudin, V. N. Staroverov, R. Kobayashi, J. Normand, K. Raghavachari, A. Rendell, J. C. Burant, S. S. Iyengar, J. Tomasi, M. Cossi, N. Rega, J. M. Millam, M. Klene, J. E. Knox, J. B. Cross, V. Bakken, C. Adamo, J. Jaramillo, R. Gomperts, R. E. Stratmann, O. Yazyev, A. J. Austin, R. Cammi, C. Pomelli, J. W. Ochterski, R. L. Martin, K. Morokuma, V. G. Zakrzewski, G. A. Voth, P. Salvador, J. J. Dannenberg, S. Dapprich, A. D. Daniels, Farkas, J. B. Foresman, J. V. Ortiz, J. Cioslowski and D. J. Fox, *Gaussian 09, Revis. B.01, Gaussian, Inc., Wallingford CT*, 2009, 1–20.
- 63 H. A. Bent, *Chem. Rev.*, 1961, **61**, 275–311.
- 64 J. A. Pople and D. P. Santry, *Mol. Phys.*, 1964, **8**, 1–18.
- 65 M. L. Clarke and J. J. R. Frew, *Organomet. Chem.*, 2009, **44**, 19–46, and references therein.
- 66 M. L. Clarke, D. J. Cole-Hamilton, A. M. Z. Slawin and J. D. Woollins, *Chem. Commun.*, 2000, 2065–2066.
- 67 P. W. Dyer, J. Fawcett, M. J. Hanton, R. D. W. Kemmitt, R. Padda and N. Singh, *J. Chem. Soc., Dalt. Trans.*, 2003, 104–113.
- 68 O. Diebolt, G. C. Fortman, H. Clavier, A. M. Z. Slawin, E. C. Escudero-Adán, J. Benet-Buchholz and S. P. Nolan, *Organometallics*, 2011, **30**, 1668–1676.
- 69 A. L. Rheingold and S. J. Geib, *Acta Crystallogr.*, 1987, **C43**, 784–786.
- 70 C. H. Suresh and N. Koga, *Inorg. Chem.*, 2002, **41**, 1573–1578.
- 71 J. Mathew and C. H. Suresh, *Organometallics*, 2011, **30**, 1438–1444.
- 72 N. M. Scott, H. Clavier, P. Mahjoor, E. D. Stevens and S. P. Nolan, *Organometallics*, 2008, **27**, 3181–3186.
- 73 D. G. Gusev, *Organometallics*, 2009, **28**, 6458–6461.
- 74 R. Dorta, N. M. Scott, C. Costabile, L. Cavallo, C. D. Hoff and S. P. Nolan, *J. Am. Chem. Soc.*, 2005, **127**, 2485–2495.
- 75 T. Lu and F. Chen, *J. Comput. Chem.*, 2012, **33**, 580–592.
- 76 J. P. Wolfe, R. A. Singer, B. H. Yang and S. L. Buchwald, *J. Am. Chem. Soc.*, 1999, **121**, 9550–9561.
- 77 T. E. Barder, S. D. Walker, J. R. Martinelli and S. L. Buchwald, *J. Am. Chem. Soc.*, 2005, **127**, 4685–4696.
- 78 *Rigaku Oxford Diffraction, CrysAlisPro Softw. Syst. 2018.*
- 79 G. M. Sheldrick, *Acta Crystallogr. Sect. A Found. Crystallogr.*, 2008, **64**, 112–122.
- 80 G. M. Sheldrick, *Acta Crystallogr. Sect. A Found. Crystallogr.*, 2015, **71**, 3–8.
- 81 O. V. Dolomanov, L. J. Bourhis, R. J. Gildea, J. A. K. Howard and H. Puschmann, *J. Appl. Crystallogr.*, 2009, **42**, 339–341.
- 82 Mathematica, version 12.0, Wolfram Res. Inc. Champaign, Illinois, 2010.
- 83 W. Humphrey, A. Dalke and K. Schulten, *J. Mol. Graph.*, 1996, **14**, 33–38.